scenario, these models are stuck on one of the steps of the staircase, partway along the transition to irregular behavior. Furthermore, these results show how a large body of modeling and theory on simpler versions of ENSO carries over to the case of complex behavior: The basic characteristics of El Niño do not depend on the seasonal cycle—but its chaotic behavior does.

REFERENCES AND NOTES

1. E. M. Rasmusson and T. H. Carpenter, *Mon. Weather Rev.* **110**, 354 (1982); M. A. Cane, *Science* **222**, 1189 (1983); E. M. Rasmusson and J. M. Wallace, *ibid.*, p. 1195; S. G. H. Philander, *Nature* **302**, 295 (1983).
2. S. G. H. Philander, *El Niño, La Niña, and the Southern Oscillation* (Academic Press, San Diego, CA, 1990).
3. J. D. Neelin, M. Latif, F.-F. Jin, *Annu. Rev. Fluid Mech.* **26**, 617 (1994).
4. E. Tziperman, L. Stone, M. A. Cane, H. Jarosh, *Science* **264**, 72 (1994).
5. F.-F. Jin and J. D. Neelin, *J. Atmos. Sci.* **50**, 3477 (1993); J. D. Neelin and F.-F. Jin, *ibid.*, p. 3504; F.-F. Jin and J. D. Neelin, *ibid.*, p. 3523.
6. The model of (*5*) has been modified to include the observed seasonal heat flux and wind stress [F.-F. Jin, J. D. Neelin, M. Ghil, *Proceedings of the Ninth Conference on Atmospheric and Oceanic Waves and Stability*, San Antonio, TX, 10 to 14 May 1993 (American Meteorological Society, Boston, 1993)].
7. M. A. Cane and S. E. Zebiak, *Science* **228**, 1084 (1985); S. E. Zebiak and M. Cane, *Mon. Weather Rev.* **115**, 2262 (1987); M. Cane, S. E. Zebiak, S. C. Dolan, *Nature* **321**, 827 (1986); T. Barnett *et al.*, *Science* **241**, 192 (1988).
8. P. S. Schopf and M. J. Suarez, *J. Atmos. Sci.* **45**, 549 (1988); Y. Wakata and E. S. Sarachik, *ibid.* **48**, 2060 (1991).
9. D. S. Battisti and A. C. Hirst, *ibid.* **46**, 1687 (1989).
10. S. G. H. Philander, R. C. Pacanowski, N. C. Lau, M. J. Nath, *J. Clim.* **5**, 308 (1992); N. C. Lau, S. G. H. Philander, M. J. Nath, *ibid.*, p. 284; P. R. Gent and J. J. Tribbia, *ibid.* **6**, 1843 (1993); G. A. Meehl, *ibid.* **3**, 72 (1990); T. Nagai, T. Tokioka, M. Endoh, Y. Kitamura, *ibid.* **5**, 1202 (1992); M. Latif, A. Sterl, E. Maier-Reimer, M. M. Junge, *ibid.* **6**, 5 (1993).
11. D. L. T. Anderson and J. P. McCreary, *J. Atmos. Sci.* **42**, 615 (1985); T. P. Barnett *et al.*, *J. Clim.* **6**, 1545 (1993); H.-H. Syu, J. D. Neelin, W. Weibel, D. Gutzler, *Extended Abstract Volume, Fourth Symposium on Global Change Studies*, Anaheim, CA, 17 to 22 January 1993 (American Meteorological Society, Boston, 1993); D.-H. Wu, D. L. T. Anderson, M. K. Davey, *J. Clim.* **6**, 1703 (1993).
12. J. D. Neelin *et al.*, *Clim. Dyn.* **7**, 73 (1992).
13. M. J. Suarez and P. S. Schopf, *J. Atmos. Sci.* **45**, 3283 (1988).
14. M. Münnich, M. Cane, S. E. Zebiak, *ibid.* **48**, 1238 (1991).
15. G. K. Vallis, *Science* **232**, 243 (1986); G. K. Vallis, *J. Geophys. Res.* **93**, 13979 (1988).
16. N. E. Graham and W. B. White, *Science* **240**, 1293 (1988).
17. M. Latif, A. Sterl, E. Maier-Reimer, M. M. Junge, *J. Clim.* **6**, 700 (1993).
18. M. H. Jensen, P. Bak, T. Bohr, *Phys. Rev. A* **30**, 1960 (1984); P. Bak, *Phys. Today* **1986**, 38 (December 1986); _____ and R. Bruinsma, *Phys. Rev. Lett.* **49**, 249 (1982); D. G. Aronson, M. A. Chory, G. R. Hall, R. P. McGehee, *Commun. Math. Phys.* **83**, 303 (1982); M. J. Feigenbaum, L. P. Kadanoff, S. J. Schenker, *Physica D* **5**, 370 (1982).
19. In Fig. 1A, we varied μ with δ_s to keep the system in the range in which a large number of Arnold tongues may be detected; this range lies quite close to the primary bifurcation. The detection of additional tongues is easier in cases with a reduced amplitude of the annual cycle, where the steps widen less rapidly with μ.
20. With the use of Floquet theory [for example, G. Iooss and D. D. Joseph, *Elementary Stability and Bifurcation Theory* (Springer-Verlag, New York, 1990); see (*6*)].
21. M. J. Feigenbaum, *J. Stat. Phys.* **19**, 25 (1978); B. Legras and M. Ghil, *J. Méc. Théor. Appl.*, numéro spécial, 45 (1983).
22. E. M. Rasmusson, X. Wang, C. F. Ropelewski, *J. Mar. Syst.* **1**, 71 (1990); C. L. Keppenne and M. Ghil, *J. Geophys. Res.* **97**, 20449 (1992).
23. N. Jiang, J. D. Neelin, M. Ghil, *Proceedings of the 17th Climate Diagnostics Workshop*, Norman, OK, 19 to 23 October 1992 (Climate Analysis Center, Washington, DC, 1993).
24. T. P. Barnett, *J. Clim.* **4**, 269 (1991).

25. We thank J. Weiss for useful references and W. Weibel for graphics. Supported in part by National Science Foundation grants ATM-9215090, ATM-9013217, and ATM-9312888; National Oceanic and Atmospheric Administration grant NA26GP0114-01; and Digital Equipment Corporation grant 1243.

29 October 1993; accepted 31 January 1994

El Niño Chaos: Overlapping of Resonances Between the Seasonal Cycle and the Pacific Ocean-Atmosphere Oscillator

Eli Tziperman,* Lewi Stone, Mark A. Cane, Hans Jarosh

The El Niño–Southern Oscillation (ENSO) cycle is modeled as a low-order chaotic process driven by the seasonal cycle. A simple model suggests that the equatorial Pacific ocean-atmosphere oscillator can go into nonlinear resonance with the seasonal cycle and that with strong enough coupling between the ocean and the atmosphere, the system may become chaotic as a result of irregular jumping of the ocean-atmosphere system among different nonlinear resonances. An analysis of a time series from an ENSO prediction model is consistent with the low-order chaos mechanism.

El Niño (roughly defined as the warming of the east equatorial water of the Pacific Ocean about every 3 to 6 years) and the accompanying Southern Oscillation signal in the atmosphere dramatically affect the Earth's climate on a global scale. The onset, termination, and cyclic nature of the ENSO events seem to be well explained by the linear equatorial wave dynamics and the delay oscillator idea (*1–5*). However, their irregular occurrence and partial locking to the regular seasonal cycle [El Niño events usually peak in the northern winter (*6*)] have been difficult to explain.

Here we use a simple delay equation model, including idealized seasonal forcing, to evaluate whether ENSO might be a low-order chaotic process driven by the seasonal cycle. We then analyze the chaotic behavior of the ENSO model of Cane and Zebiak [(*7*), hereafter CZ]. A companion paper (*8*) describes another test of this theory that uses a model that is fuller than our simple delay model and yet simpler (and therefore more accessible) than the CZ model from which we analyze a time series here.

The delay oscillator mechanism can be described as follows: A positive sea-surface temperature (SST) perturbation along the eastern equatorial Pacific weakens the easterly winds above the equator [the Bjerknes hypothesis (*9*)]. The change in the winds excites a downwelling (deepening) wave in the thermocline that travels eastward to the South American coast as equatorial Kelvin waves and an upwelling signal that travels westward as equatorial Rossby waves. The downwelling Kelvin waves enhance the warming off the coast of South America—the El Niño event has begun. Subsequently, the westward-traveling upwelling Rossby waves are reflected from the western boundary of the Pacific Ocean as upwelling Kelvin waves, which travel eastward to counter the downwelling Kelvin waves, ultimately terminating the El Niño event.

We used a simple heuristic model of this accepted delay mechanism, including a Kelvin wave, one Rossby wave mode, and a dynamic link from mid-Pacific wind stress anomalies to these equatorial wave modes. To these we added a phenomenological seasonal forcing term representing the effects of the numerous seasonally varying features of the equatorial Pacific ocean and atmosphere, such as wind amplitude and SST variations (*10*). Apart from the seasonal forcing term used here, our model is basically a continuous version of the discrete delay equation given in (*5*) and is similar to those of (*1–4*). The equation is written for $h(t)$, the thermocline depth deviations from seasonal depth values at the eastern boundary

E. Tziperman, L. Stone, H. Jarosh, Environmental Sciences and Energy Research, The Weizmann Institute of Science, Rehovot 76100, Israel.
M. A. Cane, Lamont-Doherty Earth Observatory, Columbia University, Palisades, NY 10964, USA.

*To whom correspondence should be addressed.

$$\frac{dh(t)}{dt} = aA(h\{t - [L/(2C_K)]\}) - bA(h\{t - [L/C_K + L/(2C_R)]\}) + c\cos(\omega_a t) \quad (1)$$

where t is time, L is the basin width, and ω_a is the annual frequency of the idealized seasonal forcing. The first term on the right represents a wind-forced Kelvin mode that travels at a speed C_K, and thus takes a time $L/(2C_K)$ to reach the eastern boundary from the middle of the basin. The second term is due to the westward-traveling Rossby wave of speed C_R excited by the wind at time $t - [L/C_K + L/(2C_R)]$ and reflected as a Kelvin wave.

The function $A(h)$ relates wind stress to SST and SST to thermocline depth. The nonlinear form of $A(h)$ [as in (*5*), equation 9] reflects the non-uniform stratification of the ocean. The slope of $A(h)$ at $h = 0$, set by the parameter κ, is a measure of the strength of the coupling between ocean and atmosphere (*11*).

As the nonlinearity (as measured by κ) is increased, the model follows the universal quasi-periodicity route to chaos (Fig. 1) (*12*). For small values of κ, the model time series is perfectly periodic at the annual period of the forcing (Fig. 1A, upper panel). The phase-space trajectory degenerates to a single point because of the sampling at the annual frequency (Fig. 1A, middle panel), and the power spectrum shows a single peak at the annual frequency (Fig. 1A, lower panel).

As κ increases (Fig. 1B), a second frequency (ω_n) arises, that of the natural oscillator of the Pacific ocean-atmosphere system (*1–5*). This second frequency is, in general, incommensurate with the annual frequency; the superposition of two incommensurate frequencies creates a quasi-periodic time series. The resulting oscillations are irregular but not chaotic (Fig. 1B, upper panel); the phase-space reconstruction is a simple closed loop (Fig. 1B, middle panel) (*12*), and the power spectrum shows two dominating frequencies ($\omega_n = 0.29$ and the annual $\omega_a = 1$ year^{-1}) with many subharmonics (Fig. 1B, lower panel). These irregular oscillations are not locked to the seasonal cycle.

For even stronger nonlinearity (Fig. 1C), the system becomes mode-locked: The frequency of the nonlinear delay oscillator changes slightly to a simple rational multiple of the driving annual frequency: $\omega_n = \omega_a P/Q$, with P and Q integers (in Fig. 1C, $\omega_n = \omega_a/4$). This model state corresponds to a nonlinear resonance between the driving annual frequency (ω_a) and the natural oscillator frequency (ω_n). The time series is periodic, and the phase-space diagram is a set of points whose number depends on the values of P and Q. The parameter regimes corresponding to the mode-locked solutions are also known as "Arnold tongues" (*12*).

Finally, for sufficiently large nonlinearity, the system becomes chaotic (Fig. 1D). The time series is irregular, the phase-space reconstruction is of a strange attractor, and the power spectrum is broad and not made of distinct peaks as before. For small nonlinearity, the model solution may be either quasi-periodic or mode-locked to a single nonlinear resonance defined by a single ratio P/Q. For larger nonlinearity, two or more mode-locked solutions (that is, solutions with different ratios P_i/Q_i) may coexist; the nonlinear resonances are said to overlap in this case. The chaotic behavior is caused by the irregular jumping of the system among the different possible resonances (*12*). The quasi-periodicity route to chaos is a two-parameter route. One parameter governs the transition from quasi-periodicity to chaos as shown above; the second parameter governs the width of the mode-locked regimes, as investigated by Jin *et al.* (*8*).

We suggest that ENSO characteristics may be consistent with low-order chaotic behavior of the type described (Fig. 1D), which would account for ENSO's irregularity and its locking to the seasonal cycle. Each mode-locked solution (Fig. 1C) is in perfect phase correlation with the driving annual frequency. But even in the chaotic regime, as the system jumps irregularly among resonances, it remains partially locked to the

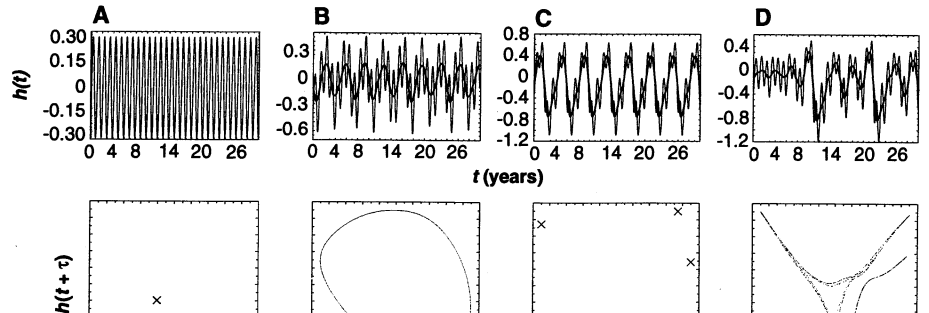

Fig. 1. The transition to chaos of the delay model. The data for these plots were obtained by running Eq. 1 for 1024 years to remove all transients and then for 1024 more years to obtain the data for the analyses. Shown are a time series of the model results (upper panels, thin lines), together with a 12-month running average of these results (upper panels, thick lines); a phase-space diagram (middle panels); and a logarithm of the power spectrum (lower panels) for the model time series. The reconstructed phase-space diagram is obtained by plotting $h(t)$ versus $h(t + \tau)$, where τ is the delay time (*19*) (not to be confused with the delay times of the delay oscillator), chosen here to be 1 year. The time series for $h(t)$ is subsampled at the frequency of the external forcing, that is, at 1-year intervals (*12*). The four cases shown are (**A**) $\kappa = 0.9$, (**B**) $\kappa = 1.2$, (**C**) $\kappa = 1.5$, and (**D**) $\kappa = 2.0$ and $b_+ = 1.5$. The few points contained in the phase-space diagram in (A) and (C) are denoted by "x."

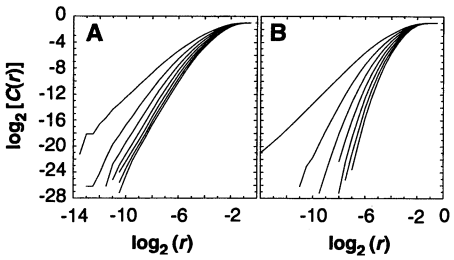

Fig. 2. Correlation dimension estimates for (**A**) the CZ model (*18*) and (**B**) the linear Markov model. Shown is a $\log_2$-$\log_2$ plot of the Grassberger-Procaccia (*15*) correlation function as a function of the distance between trajectory points in reconstructed phase space. Each curve is for a different embedding dimension d_E, with the uppermost for $d_E = 2$ and the rest for d_E increasing in steps of 2. The dimension of the attractor that produced the time series is given by the slope of the linear segment in these curves. The curves calculated for the CZ model contain a linear segment whose slope converges to a constant value as the embedding dimension increases. The dimension calculated from these curves is about 3.5. The slopes for the Markov model time series (B) do not seem to converge as quickly as those for the CZ model time series for increasing embedding dimension, which suggests instead a higher dimension, as is characteristic of randomly driven linear systems.

driving seasonal frequency: The maxima of the 12-month running average of the model time series [representing the ENSO warm events (Fig. 1D, upper panel)] occur every 2 to 5 years and always within the same 4 months of the calendar year—precisely the ENSO characteristic missing in the existing simplified delay-oscillator ENSO models. Earlier examinations of ENSO as a low-order chaotic system either have used simplified models lacking the essential equatorial wave dynamics (although they discussed the locking to the seasonal cycle) (*13*) or did not fully realize the importance of mode locking to the seasonal cycle and the mechanism of resonance overlapping (*5*).

Is the irregularity of ENSO indeed due to low-order chaos and not to random forcing (*2*)? The instrumental record of the real ENSO data, which extends over slightly more than 100 years, is too short to identify chaos in an observed time series. Instead, we analyzed the results of the CZ ENSO model (*7*), which has been used to predict several ENSO events (*14*).

The diagnostic tool we used to identify chaotic model behavior was the calculation of the phase-space correlation dimension (*15*) from monthly averaged East Pacific SST from a 1024-year run. The correlation dimension for this run is about $d \approx 3.5$ (Fig. 2A), which suggests a chaotic dynamic system with a small $[\leq(2d + 1)]$ number of degrees of freedom.

The correlation dimension calculations are prone to various artifacts (*16*), and in order to reduce this possibility we used a control time series of surrogate data (*17*) with the same characteristics (number of points, power spectrum) as the CZ model time series. We chose a time series from a linear Markov model built from the CZ model and driven by random forcing (*18*). The dimension estimate for the Markov model (Fig. 2B) indicates that this time series is random and distinguishable from the low-order dimension found with the CZ model. This result is consistent with the suggestion that the irregularity of ENSO events (at least in the CZ model) is not due to random noise (such as ocean weather phenomena present in the CZ model).

We suggest that the natural oscillator of the equatorial Pacific ocean-atmosphere system can enter into nonlinear resonance with the seasonal cycle at several periods of the oscillator (mostly 2 to 5 years). The coexistence of these resonances results in chaotic behavior that is due to the jumping of the system among the different resonances. This is a feature of the quasi-periodicity route to chaos (*12*).

Much additional work is needed to further examine the relevance of these ideas to the observed ENSO characteristics and to clarify the spatial and temporal mechanisms of the seasonal forcing of Pacific interannual variability. If this theory can be validated, the ENSO cycle might be established as an example of low-order chaos in a highly complex physical system.

REFERENCES AND NOTES

1. M. J. Suarez and P. S. Schopf, *J. Atmos. Sci.* **45**, 3283 (1988).
2. N. E. Graham and W. B. White, *Science* **240**, 1293 (1988).
3. D. S. Battisti and A. C. Hirst, *J. Atmos. Sci.* **46**, 1687 (1989).
4. M. A. Cane, M. Munnich, S. E. Zebiak, *ibid.* **47**, 1562 (1990).
5. M. Munnich, M. A. Cane, S. E. Zebiak, *ibid.* **48**, 1238 (1991).
6. E. Rasmusson and T. Carpenter, *Mon. Weather Rev.* **110**, 354 (1982).
7. M. A. Cane and S. E. Zebiak, *Science* **228**, 1085 (1985); S. E. Zebiak and M. Cane, *Mon. Weather Rev.* **115**, 2262 (1987).
8. F.-F. Jin, J. D. Neelin, M. Ghil, *Science* **264**, 70 (1994).
9. J. Bjerknes, *Mon. Weather Rev.* **97**, 163 (1969).
10. S. G. Philander, *El Niño, La Niña, and the Southern Oscillations* (Academic Press, San Diego, CA, 1990).
11. The model parameters are $C_K = L/(2.3$ months), $C_R = C_K/3$, $a = 1/(180$ days), $b = 1/(120$ days), and $c = 1/(138$ days). Unless indicated otherwise, $A(h)$ is as in (*5*) with $a_+ = 1$, $a_- = 1$, $b_+ = 2.0$, and $b_- = -b_+/5$. Our heuristic model equation produces regular ENSO oscillations when run without the seasonal forcing term. Equation 1 was integrated by use of a high-accuracy, variable-order, variable-step Adams method using routine D02CBF in *Fortran Library Manual, Mark II* (Numerical Algorithms Group, 1984).
12. P. Bak, T. Bohr, M. H. Jensen, *Phys. Scr.* **T9**, 50 (1985); T. Bohr, P. Bak, M. H. Jensen, *Phys. Rev. A* **30**, 1970 (1984).
13. G. K. Vallis, *Science* **232**, 243 (1986); *J. Geophys. Res.* **93C**, 13979 (1988).
14. M. A. Cane, S. E. Zebiak, S. C. Dolan, *Nature* **321**, 827 (1986).
15. P. Grassberger and I. Procaccia, *Physica D* **9**, 189 (1983).
16. J.-P. Eckmann and D. Ruelle, *ibid.* **56**, 185 (1992).
17. J. Theiler, B. Galdrikian, A. Longtin, S. Eubank, J. D. Farmer, in *Nonlinear Prediction and Modeling*, M. Casdagli and S. Eubank, Eds. (Addison Wesley, Redwood City, CA, 1991), pp. 163–188. The number of model data points used to obtain Fig. 2 is sufficient to determine the correlation dimension of the system based on the theoretical limitations given in (*16*). In contrast, a real ENSO time series of 100 years at most is probably too short for the dimension estimate.
18. M. A. Cane, S. E. Zebiak, Y. Xue, Eds., *Proceedings of the Workshop on Decade to Century Time Scales of Natural Climate Variability*, Climate Research Committee, National Academy of Sciences, Irvine, CA, 21 to 24 September 1992 (National Academy Press, Washington, DC, in press).
19. A. M. Fraser and H. L. Swinney, *Phys. Rev. A* **33**, 1134 (1986).

20. We thank M. Munnich and Y. Xue for their help. M.A.C. was supported by grant NA16-RC-0432-03 from the National Oceanic and Atmospheric Administration and grant OCE-90-00127 from NSF.

1 July 1993; accepted 31 January 1994

Growth of Continental-Scale Metro-Agro-Plexes, Regional Ozone Pollution, and World Food Production

W. L. Chameides,* P. S. Kasibhatla,† J. Yienger, H. Levy II

Three regions of the northern mid-latitudes, the continental-scale metro-agro-plexes, presently dominate global industrial and agricultural productivity. Although these regions cover only 23 percent of the Earth's continents, they account for most of the world's commercial energy consumption, fertilizer use, food-crop production, and food exports. They also account for more than half of the world's atmospheric nitrogen oxide (NO_x) emissions and, as a result, are prone to ground-level ozone (O_3) pollution during the summer months. On the basis of a global simulation of atmospheric reactive nitrogen compounds, it is estimated that about 10 to 35 percent of the world's grain production may occur in parts of these regions where ozone pollution may reduce crop yields. Exposure to yield-reducing ozone pollution may triple by 2025 if rising anthropogenic NO_x emissions are not abated.

The unprecedented increase in the standard of living of humanity since the Industrial Revolution can be attributed in part to two factors: the development of high-input–high-yield agriculture, capable of feeding an increasingly urban population, and an urban-industrial infrastructure, heavily dependent on fossil fuels for the production and transport of manufactured goods (*1*). The correlation between agriculture and fossil fuel burning is most pronounced in three regions of the northern mid-latitudes (Fig. 1): (i) eastern North America (25° to 50°N and 105° to 60°W); (ii) Europe (36° to 70°N and 10°W to 90°E); and (iii)

W. L. Chameides and P. S. Kasibhatla, School of Earth and Atmospheric Sciences, Georgia Institute of Technology, Atlanta, GA 30332, USA.
J. Yienger and H. Levy II, Geophysical Fluid Dynamics Laboratory, Princeton University, Princeton, NJ 08542, USA.

*To whom correspondence should be addressed.
†Visiting scientist at Geophysical Fluid Dynamics Laboratory, Princeton University, Princeton, NJ 08542, USA.